NUMERICAL SIMULATION OF THE 1918 PUERTO RICO TSUNAMI

A. Mercado[1], and W. McCann[2]
[1]*Department of Marine Sciences, University of Puerto Rico, P.O. Box 9013, Mayaguez, P.R. 00680*
E-mail: a_mercado@rumac.upr.clu.edu
[2]*Earth Scientific Consultants, 6860 West 99th Avenue, Westminter, CO 80021*
E-mail: esc@envisionet.net

Abstract. The Caribbean Sea region is well known for its hurricanes, and less known for tsunamis. As part of its responsibilities in hazard assessment and mitigation, the U.S.A. Federal Emergency Management Agency, and the Puerto Rico Civil Defense, funded a pilot study to perform a numerical simulation of the 1918 Puerto Rico tsunami, one of the most deadly in the region. As part of the study a review has been made of the tectonic and tsunamigenic environment around Puerto Rico, the fault parameters for the 1918 event have been estimated, and a numerical simulation has been done using a tsunami propagation and runup model obtained through the Tsunami Inundation Modeling for Exchange (TIME) program. Model results have been compared with the observed runup values all along the west coast of Puerto Rico.

Keywords: tsunamis, historical earthquakes, risk assessment, Caribbean Sea

1. INTRODUCTION

The Caribbean Sea region is well known for its hurricanes, but is not known for another major threat that is mostly associated with other oceans and seas, and that is tsunamis. But the historical fact is that tsunamis are a reality in the Caribbean Sea region. Although much more rarer than hurricanes, its life-threatening potential is such that, on a death toll basis, they are comparable to hurricanes. As a matter of fact, Lander (1997) has shown that the amount of deaths associated with tsunamis in the Caribbean since 1500 are greater than the sum of all of the tsunami-related deaths in Alaska, Hawaii, and the western seaboard of the United States of America.

One of the most deadly tsunamis ever in the Caribbean Sea Region occurred in October 11, 1918. It was a local, earthquake-related, tsunami which affected mainly the west coast of the island of Puerto Rico (see Figure 1), and whose impact was well documented in a U.S. Congress report (Reid and Taber, 1919). Federal and local authorities are concerned about the possibility of this happening again, specially now that the coastal population has increased enormously. For this reason they have been funding a series of projects with the ultimate objective of mapping the tsunami flooding threat all along Puerto Rico. It is the purpose of this article to present the results of a numerical simulation of this event, and how it did compare with the observations. This was a pilot study made with the purpose of ascertaining the usefulness of tsunami simulations, including runup, in mapping the tsunami hazard in the island of Puerto Rico.

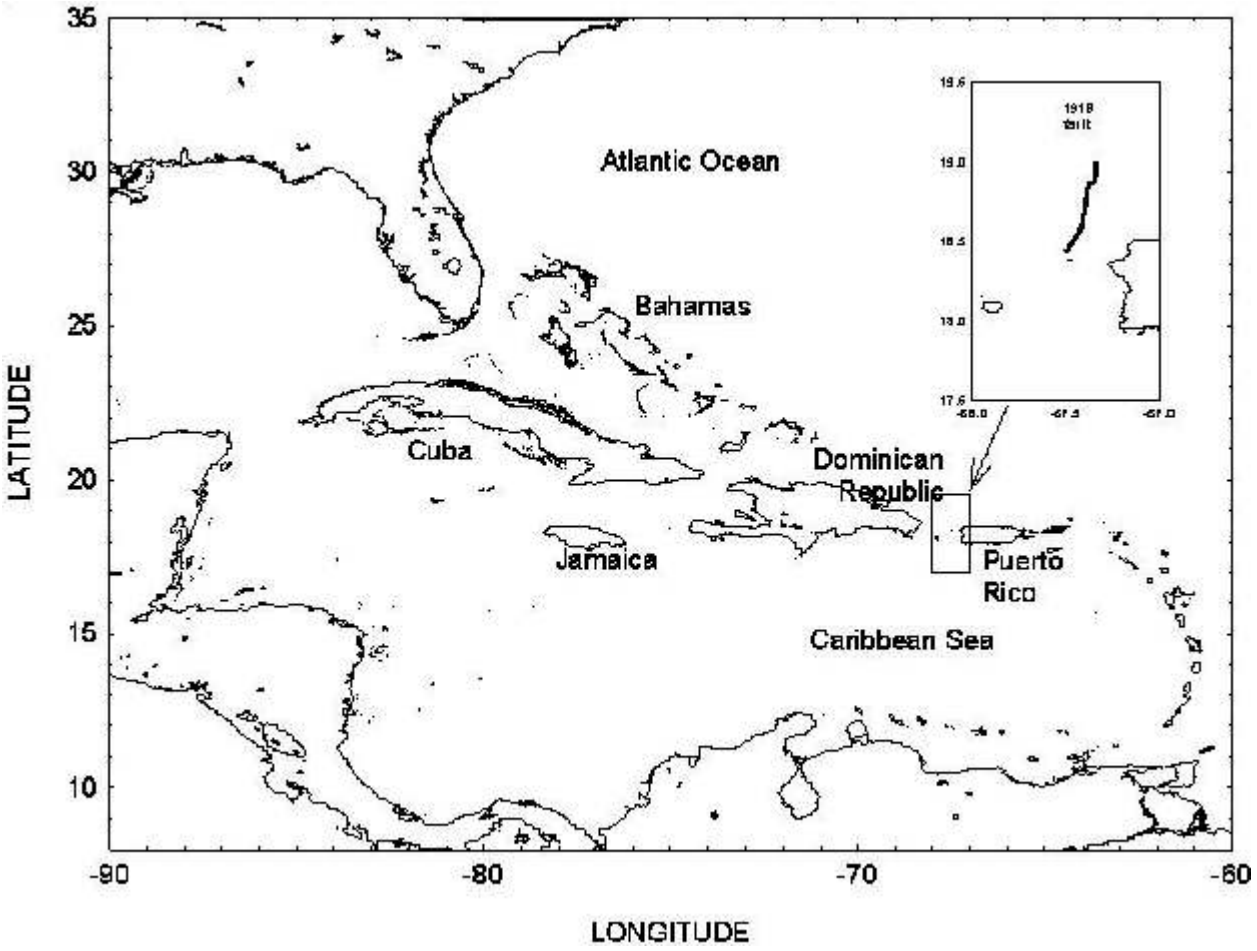

Figure 1 Location map of study site. Insert shows location of fault that generated the 1918 tsunami.

2. TECTONIC AND TSUNAMIGENIC ENVIRONMENT OF PUERTO RICO

The northeastern portion of the Caribbean Plate is the general tectonic setting for Puerto Rico. The island lies within the East-West trending Plate Boundary Zone (PBZ) between the generally westward moving North American Plate and the Eastward moving Caribbean Plate (Fig. 2). In detail, these relative movements include a significant, observable component of convergence. That is, with respect to a fixed Caribbean Plate, the North American Plate moves in a West-Southwest direction (Sykes et al., 1982; Deng and Sykes, 1995). The oblique nature of the relative plate motion is associated with a complex set of secondary movements occurring along a narrow plate boundary zone. Identification of several integral units or platelets within the PBZ has led to the development of numerous models to define their margins and to explain their motions (Byrne et al., 1985; Masson and Scanlon, 1991).

The rate of relative movement of the larger plates has been estimated by many researchers. These

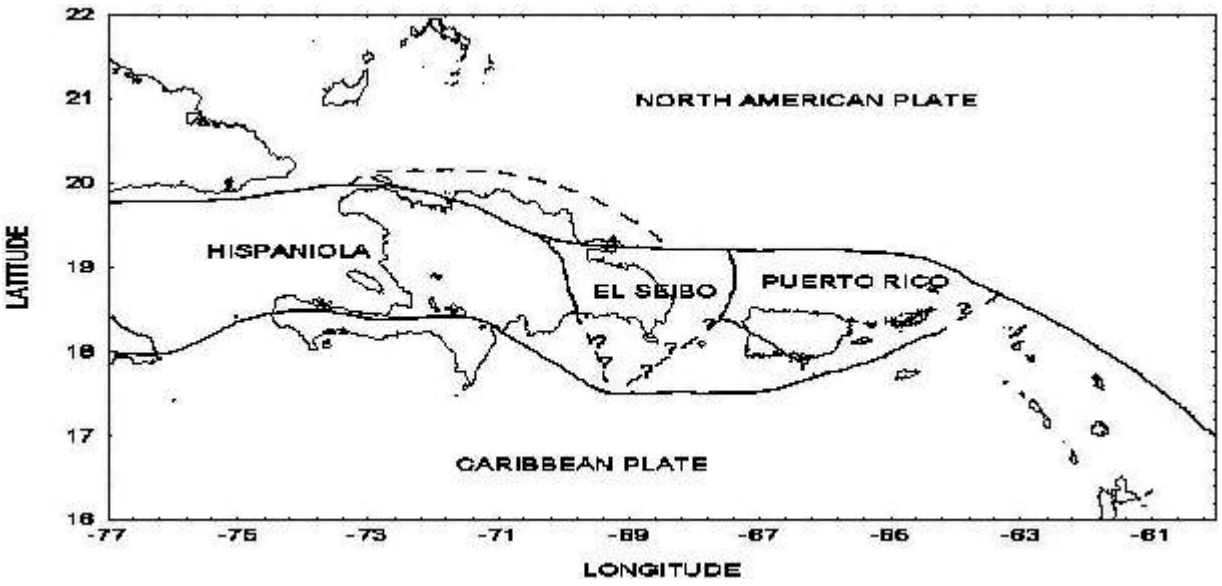

Figure 2 Location of presently identified plates, platlets, and tectonic blocks in the Plate Boundary Zone separating the Caribbean and North American Plates.

estimates vary by a factor of two, from less than 20 mm/yr (DeMets, 1993) to about 37 mm/yr (Sykes et al., 1982). The rates and exact directions of interblock movements within the PBZ are less precisely known, with researchers not even agreeing on the general styles of motion. The Puerto Rico platelet is the easternmost of the blocks in the PBZ. It is bounded by four margins or tectonic elements (Figure 2). To the north lies the subduction zone where the North American Plate descends into the mantle at the Puerto Rico Trench, to the south the

platelet abuts the subduction zone of the Caribbean Plate. To the east and southeast is the extensional Anegada Passage, to the west is the ill-defined zone separating the western part of the island of Puerto Rico from the El Seibo block in the Dominican Republic. Along each of these margins the zone of contact is likely to be complex, with many terranes or smaller slivers juxtaposed in the actual zone of contact.

The complex motions near Northwestern Puerto Rico include extension in the Mona Canyon and in other parts of the Mona Passage (which separates western Puerto Rico from eastern Hispaniola, or Dominican Republic) to the south, oblique thrusting and possible strike-slip motion in the Puerto Rico Trench to the North. The most important features with tsunami generating potential are the large faults in the Mona Canyon and the northern part of the Mona Passage.

3. TSUNAMIGENIC SOURCES NEAR NORTHWESTERN PUERTO RICO

The most important tsunamigenic sources near northwestern Puerto Rico are those associated with the Mona Canyon. That feature is a narrow, deep depression in the inner wall of the Puerto Rico trench (Figure 3.). In several areas the floor of the canyon lies more than 2 km lower than

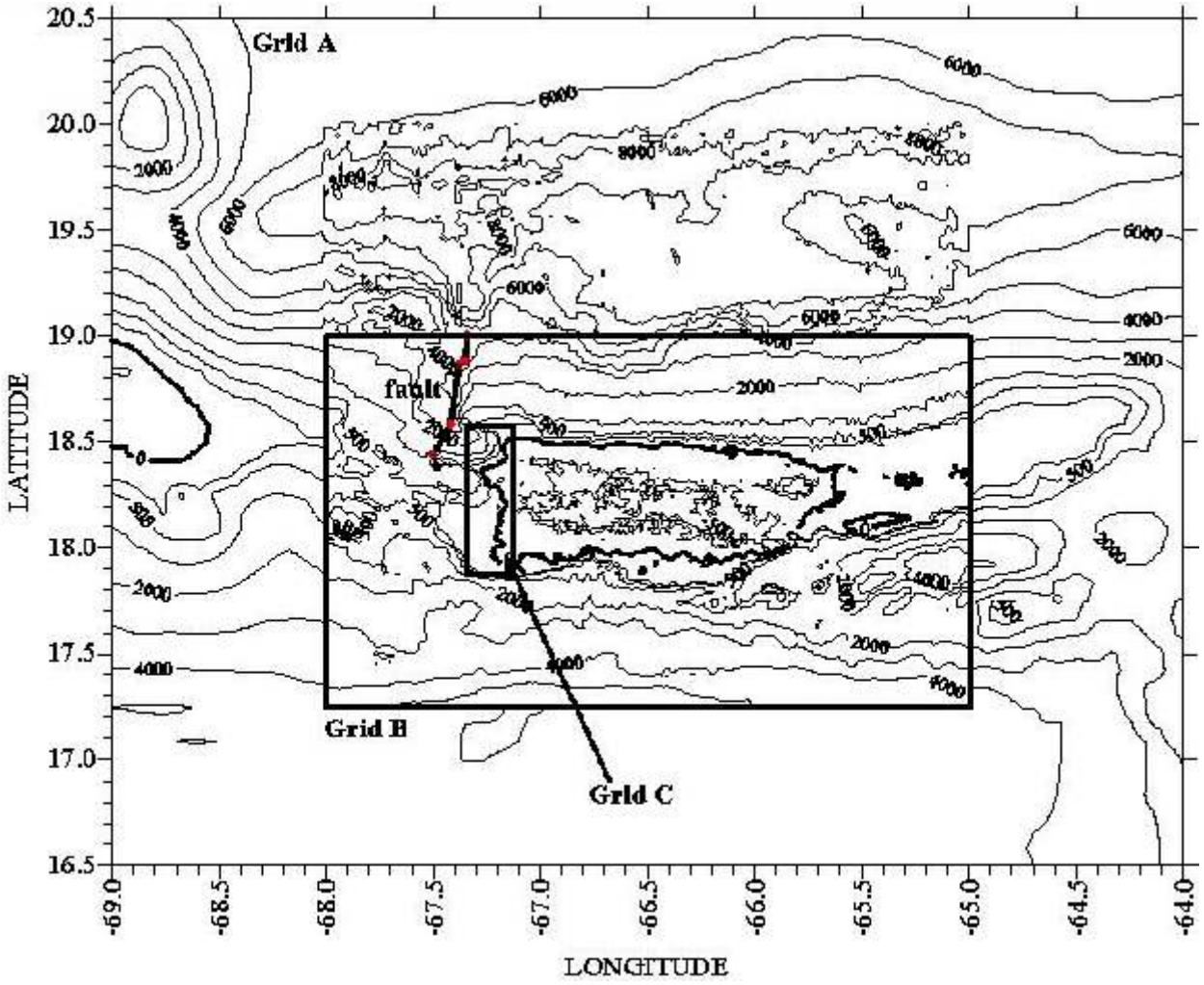

Figure 3 Bathymetric nested grid maps (see Table I). Also shown is the source fault along the eastern slope of the Mona Canyon. Depths are in meters.

the surrounding seafloor. The difference in water depth is due to the large scale down dropping of blocks of the inner wall of the trench by extensional tectonics and resulting development of normal faults. Western Geophysical, Lamont Doherty Earth Observatory, United States Geological Service and oceanographic institutions have collected seismic reflection lines for the Mona Canyon area. Those reflection lines provide images of the subsurface of the seafloor, displaying the location of active faults and the nature of movements on them. Figure 3 shows the bathymetry of the Mona Canyon region. It is clear that this feature dominates the submarine structures off northwestern Puerto Rico. Figure 4 shows the locations of faults known to cut the lowest observable rock layers in the various seismic reflection lines as proposed by Western Geophysical (1973) . The faults in Figure 4 are those considered to be active as a result of reinterpretation of the Western Geophysical and other seismic reflection data. These faults are being used in the development of tsunami hazard flood maps for western Puerto Rico.

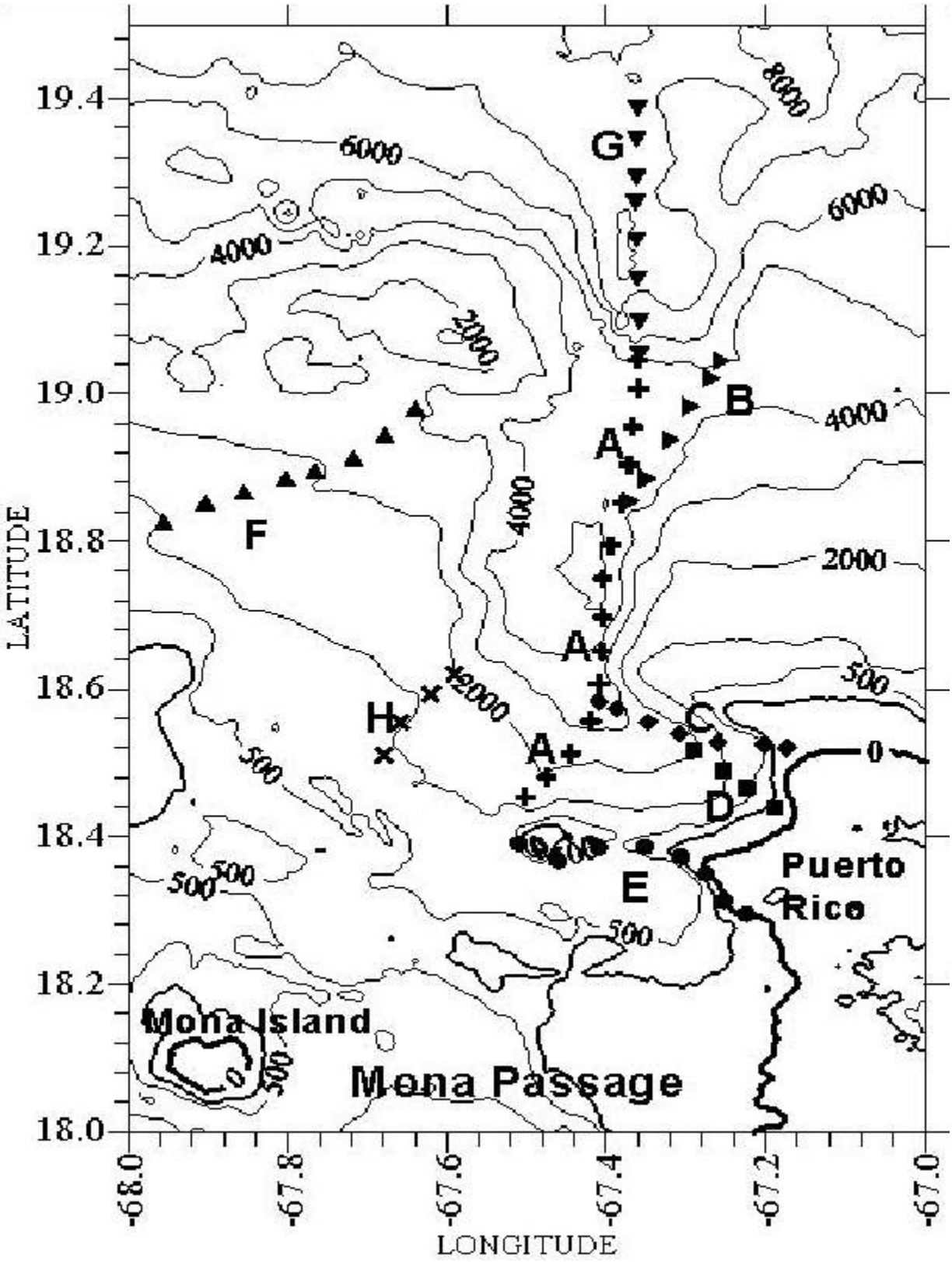

Figure 4 Location of principal faults based on seismic rflection records (Western Geophysical) in Mona Canyon region.

4. THE 1918 PUERTO RICO TSUNAMI

On October 11, 1918 at 10:14 in the morning, a magnitude 7.3 earthquake occurred about 15 km off the northwest coast of Puerto Rico. It generated a large tsunami that caused damage at various points along the western and northern coasts of the island. Maximum tsunami runup of 6 meters were reported. 116 persons perished, with about 40 dying because of the tsunami. The following is taken directly from Reid and Taber (1919), and the location of referenced sites can be seen in Figure 7, together with the observed runup: "The great sea wave which followed the earthquake of October 11 was the highest at points near the northwest corner of Puerto Rico, where it was observed almost immediately after the earthquake. In passing along the coast toward the south and toward the east, the wave decreased in height, though not uniformly, and the time interval between the earthquake shock and the arrival of the sea wave gradually increased. Wherever the wave was seen along the coasts of Puerto Rico observers report that the ocean first withdrew from the land, in places exposing reefs and stretches of sea bottom never visible during the lowest tides, and then the water returned reaching heights that were equally high above normal. At some places the great wave was followed by one or more smaller ones, especially in sheltered bays, the water continued to ebb and flow for some time."

"At the Punta Borinquen Lighthouse the keeper, who was up in the tower when the earthquake began, immediately started down the stairs, and as he went down he noticed that the water along the shore had already begun to recede. It returned quickly, and measurements to points indicated by him show that the height reached by the water, not counting the wash of the wave, was about 4.5 meters above mean sea level. Just southwest of the lighthouse, where the land is lower, the water is reported to have washed inland 100 m into a grove of coconut palms. The lighthouse keeper had the impression that the wave came from the northwest."

"Near Punta Agujereada the limestone cliffs are 100-120 m in height, and at their base there is a narrow strip of beach which, in the wider places, was planted with coconut palms and was also used for pasturage. Several hundred palms were uprooted by the wave, and the beach was turned into a sandy waste. In this vicinity a few small houses were destroyed, and eight people are reported to have been drowned. Several persons visiting the district soon after the occurrence estimated the height of the wave as 5.5-6 m and the evidence remaining at the time of our visit supported these estimates."

"At many places we were able to make fairly accurate measurements of the height of the wave, as the water had entered the ground floors of houses, staining wall paper and leaving a record that was plainly visible for a long time afterwards. At Aguadilla the height of the wave seems to have varied somewhat in different parts of the city, but at no place were the measurements less than 2.4 m above sea level. and near the head of the bay the crest of the wave must have been at least 3.4 m in height. In this town 32 people are said to have been drowned, and about 300 little huts built along the beach were destroyed. Estimates of the time interval between the earthquake shock and the arrival of the sea wave made by different observers, range from 4 to 7 minutes, one of the best being 5 to 6 minutes. The calculated time for the wave to travel from the earthquake origin to Aguadilla is 5 minutes."

"The Columbus Monument, which stood on the beach near the mouth of the Culebrinas River, about 4 km southwest of Aguadilla, was thrown down probably by the earthquake and rectangular blocks of limestone weighing over a ton (1,000 kg) were carried inland and slightly downhill by the wave to (distances of 45 and 75 m). The water washed over dune sand which was 3.4 m above sea level, and the effects on vegetation indicated that the wave could not have been less than 4 m high."

"At the Punta Jiguero (Punta Higuero) lighthouse the keeper, shortly after the earthquake, saw the ocean retire from the shore; and upon returning about 2 minutes later, it uprooted coconut palms a short distance north of the lighthouse and crossed the railroad track, leaving fish between the rails which are here 5.2 m above sea level. At the time of our visit the vegetation by the track still showed marks of the rush of the water."

"At Mayaguez the sea wave entered the lower floors of buildings near the water front and destroyed a few native huts along the beach, but did comparatively little damage. A small house was carried seaward by the retiring wave and left stranded a short distance from the shore. Lighters and other small boats, anchored 300 to 400 m off shore, were not affected. In the northern part of the city a narrow brick wall running S 76 degrees E was overturned by the wave. In this vicinity the watermarks on houses indicate that the wave reached a height of 1.1 to 1.2 m above sea level; farther south in Mayaguez the height was 1.5 m. In the interval between the earthquake and the arrival of the sea wave, an automobile traveled from Central Corsica near Rincón to Mayaguez, a trip that is estimated to require 25-30 minutes. The calculated interval is about 23 minutes."

"At El Boquerón (Boquerón Bay) near the southwest corner of Puerto Rico, the wave was about a meter in height. An observer states that the ocean withdrew about an hour after the earthquake, the water going out gradually during a period of 20 minutes. The calculated interval is about 45 minutes. A small boat anchored 50 m from shore. where the water is normally 1.5 m in depth. rested on the bottom for a few minutes. The ocean returned more rapidly than it retired, and the first wave was followed by several smaller ones."

"On the west coast of Mona Island the water first retired, and after a short interval, resumed, washing away a small pier and filling and open cistern, about 4 m above sea level."

5. FAULT PARAMETERS FOR THE 1918 TSUNAMI

The location of observed active faults are shown in Figure 4. Estimates of the lengths of the principal faults and maximum magnitude of possible fault rupturing earthquake are shown in Tables 1 and 2. To maintain simplicity, the moment magnitude ($Mo=\mu WLD$) estimation method was used, assuming a rigidity of $\mu = 3x10^{11}$ N/m^2. Maximum depth of faulting (W) was assumed to be 25 km for all faults, known fault lengths (L) were related to magnitude using the relation of Slemmons and Polo (1992). Also, slip (D) was related to event moment using the relation of Slemmons and Polo (1992). Assuming all faulting continues to a constant depth will overestimate the magnitude of the shorter faults, however, this does not affect the final conclusion about maximum tsunami runup along the northwest coast.

The data shown in Table 1 (for Mona Canyon fault - A) is the one used for the numerical simulation

described here. Table 2 contains parameters for other faults in the area. The information in both tables was acquired by reinterpretation of seismic reflection lines, and analysis of a inhouse bathymetric map produced by data provided by the National Geophysical Data Center and Mercado (1994). That data set was checked for errors, and contoured. The data was analyzed for depth of seafloor, seafloor slope amplitude and direction, so as to determine the location of faulted blocks, and to the check the continuity of fault scarps observed on the various reflection lines. Letters indicating the position of the faults in Tables 1 and 2 correspond to the letters in Figure 4.

All faults noted have at least some degree of vertical slip, the North striking faults more so than the WNW trending, more transcurrent, faults to the south. The North Mona Canyon Fault (G) is an east facing normal fault connected to the west facing Mona Canyon Fault (A - also a normal fault) by a complex transfer zone near 19˚N. This fault system is thus strongly influenced by the strike-slip 19˚N fault.

The information in Tables 1 and 2 clearly demonstrate that the Mona Canyon Fault (A) is the most probable source of the 1918 earthquake. It also shows that there are at least seven other faults in the Mona Canyon region capable of generating tsunamis, although some of those appear to be shorter and, therefore, less capable than the Mona Canyon Fault System. Tsunami events larger than that of the 1918 event seem improbable given existing data.

Notice that the rake angle, λ, is negative, which implies that the so-called *hanging wall* of the fault system has a downward slip component, producing what is known as a *normal fault.*

6. BATHYMETRIC AND TOPOGRAPHIC DATA

Tsunamis are classified as shallow water, or long, waves. As such, their propagation is strongly affected by depth changes, but mainly large-scale changes. Their runup (i.e., flooding of dry coastal areas) is also dependent on the dry land (i.e., terrain above Mean Sea Level - MSL) configuration. Hence, it is important to have higher resolution as we approach the coast. This is

TABLE 1
FAULT SEGMENTS AND THEIR PARAMETERS FOR MONA CANYON FAULT (A)
(all segments are assumed to have a fault plane width, W, of 23 km,
and are labeled 1 to 4, starting with the northernmost one)

SEGMENT	END POINTS		FAULT PARAMETERS					
	Lon.	Lat.	Length (km)	Strike[1] Θ	Dip Dir. δ	Slip Dir. λ	Slip(m) (7.5)[3]	Depth[3] (m)
4	start: -67.42	start: 18.58	18	210	60	-120	4	2,309
	end: -67.50	end: 18.44			N60W			

3	start: -67.38	start: 18.86	31	188	82	-98	4	4,336
	end: -67.42	end: 18.58			N82W			
2	start: -67.35	start: 18.88	4	236	34	-146	4	4,712
	end: -67.38	end: 18.86			N34W			
1	start: -67.34	start: 19.00	13	185	85	-95	4	4,674
	end: -67.35	end: 18.88			N85W			

1 - Following the convention in Aki and Richards (1980), strike is measured from North, looking along the strike direction from the beginning of the fault
2 - Earthquake magnitude in Richter scale
3 - Average depth of segment

one of the reasons the numerical model makes use of, in this case, nested grids of sea bottom depths and terrain elevations. Therefore, it is extremely important that these depths and elevations be given as accurately as possible.

The model used in this simulation, described in the report by Goto and Ogawa (1992) works with a set of nested grids, where the grid resolution increases in the coastal areas which are to be studied in greater detail. For example, in this study three nested grids are used (Figure 3) whose relevant parameters are given in Table 3 below.

The exterior grid (A) extends past the Puerto Rico Trench along its northern boundary to allow

TABLE 2
FAULT PARAMETERS OF OTHER SIGNIFICANT
FAULTS IN THE MONA CANYON REGION

FAULT NAME	END POINTS		FAULT PARAMETERS			
	LON	LAT	LENGTH (km)	STRIKE (degrees)	DIP DIRECTION	MAX. MAGNITUDE
Mona Canyon - East Branch (B)	-67.38	18.83	22	30	NW	7
	-67.28	19.00				
Borinquen (C)	-67.40	18.58	26	105	SSW	7
	-67.17	18.52				
Borinquen - South Branch (D)	-67.31	18.56	20	135	SW	6.9

	-67.18	18.43				
Desecheo (E)	-67.5	18.38	34	107	S	7.2
	-67.21	18.29				
Taino (F)	-67.96	18.82	44	63	SE	7.4
	-67.61	19.00				
North Mona Canyon (G)	-67.36	19.11	26	178	E	7
	-67.37	19.34				
Cabeza (H)	-67.68	18.51	16	45	SE	6.9
	-67.58	18.61				

for the possibility of the tsunami wave propagating eastward along the Trench, where it will move at a faster speed due to the increased water depth. The intermediate grid (B) allows for a better resolution all around Puerto Rico. The increased resolution is essential in order to simulate as best as possible the travel time of the wave. The interior grid (C), with the highest resolution, is needed in order to make the runup calculations as accurately as possible. For the runup calculations the model has to be run in its non-linear mode (i.e., keeping the non-linear terms in the conservation of momentum equations), which requires much more CPU time than in the linear mode. For grids A and B the model is run in the linear mode which, although not good enough for runup estimates, it is good enough for travel time estimates.

Another reason for increasing the resolution as we go into shallower water is the fact that (Shuto et al., 1985, 1986) each tsunami wavelength should be covered by at least 20 grid points in order to diminish numerical dispersion (dissipation). Ramming and Kowalik (1980) found that 10 grid points per wavelength is sufficient if we are willing to accept a 2% error in the phase velocity. Still another reason is that numerical stability considerations (the CFL criteria to be discussed below) requires that the finite differences time step be such that $\Delta t \leq \Delta x/(2gh_{max})^{1/2}$, where Δx is the space discretization size, g is the gravitational acceleration, and h_{max} is the maximum depth in the given grid. As the wave propagates into shallower waters h_{max} decreases and by decreasing Δx we can maintain a constant Δt (Goto and Ogawa, 1982).

TABLE 3
PARAMETERS FOR NESTED GRIDS

Grid	Min. Lat. (˚)	Max. Lat. (˚)	Min. Lon. (˚)	Max. Lon. (˚)	No. Columns	No. Rows	Cell Size (sec of arc)	Cell Size (meters)
A	15.7550	21.0000	64.0000	69.0000	667	700	27	~ 790
B	17.2500	18.9975	65.0000	68.0000	1201	700	9	~ 263
C	17.8733	18.5758	67.1317	67.3442	256	844	3	~ 88

In this report various sources of data were used for preparing the nested grids. For grid A the source of data was the so-called ETOPO-5 data, available from the National Geophysical Data Center, which consists of digital average land and sea floor elevations assembled from several uniformly gridded data bases into a worldwide gridded data set with a grid spacing of 5 minutes of latitude by 5 minutes of longitude. This data was interpolated from its original 300 seconds of arc spacing to 27 seconds when preparing grid A.

Since the effect of the Puerto Rico Trench is expected to be important for travel time estimates along the north coast, it was decided to replace the data in the Trench with a more accurate data set. This was done by means of data supplied from a CD obtained from the National Geophysical Data Center (NGDC) based on research ship data. Therefore, the gridded, interpolated, ETOPO-5 data in the rectangle between 19˚ and 20˚ N, 65˚ to 68˚ W, was replaced with the NGDC data, and the effect of the higher resolution can be seen in Figure 3 just north of the upper boundary of grid B.

The data source for the intermediate and inner grids (B and C, respectively) is based on data that was directly digitized from National Ocean Survey so-called "smooth sheets", as part of a University of Puerto Rico Sea Grant College Program sponsored project (Mercado, 1994).

The land values were obtained from a Digital Elevation Model (DEM) for Puerto Rico (US Geological Survey), with a cell resolution of 3 seconds. This is why the inner grid, Grid C, was chosen with a grid spacing of 3 seconds.

6. THE TSUNAMI GENERATION MODEL

There are three phases in the life of a tsunami: generation, propagation, and runup. Tsunamis can be generated by various causes: earthquake submarine faults, underwater explosions from volcanoes, subaerial landslides impinging on the sea, submarine landslides. According to available evidence the 1918 west coast event was due to a submarine earthquake fault located on the Mona Canyon, approximately 24.2 km west of Punta Higuero, the westernmost tip of Puerto Rico (see Figure 7). It was what is called a near-field tsunami, because it was generated close to the affected area.

The initial condition consist of a sea surface deformation which itself, in this case, it is due to a vertical displacement of the sea bottom. In this report the vertical displacement of the sea bottom is calculated with the Mansinha and Smylie method (1972), and is assumed equal to the tsunami initial profile with no modification. This assumption is valid because the horizontal size of the initial profile is sufficiently large compared with the water depth at the tsunami source, and the rupture velocity is assumed very short compared with the tsunami propagation velocity (Shuto, 1991). Kowalik and Whitmore (1991) have shown that the consideration of a finite (versus infinite) rupture velocity (also called a moving rupture versus an instantaneous uplift) has a small effect on the energy flux distribution (or directionality) of the tsunami and on the tsunami itself.

The initial displacement is generated in the exterior domain (A), and it is interpolated into the

higher resolution grids B and C. The end result is an initial sea surface profile that extends smoothly from the exterior, lower resolution, domain into the higher resolution domains. This is the sea surface condition at time $t = 0$ seconds. That is, the hypothesis is that the sea bottom displacement is immediately reflected in a sea surface displacement.

7. THE TSUNAMI PROPAGATION AND RUNUP MODEL

The models used in this study were available through the Tsunami Inundation Modeling for Exchange (TIME) program. The model and its use are described in the report by Goto and Ogawa (1992). Long wave theory is used (where the ratio of water depth to wavelength is small), for which the vertical acceleration of water particles is negligible compared to the gravitational acceleration, and the hydrostatic pressure approximation is used. But the non-linear terms are kept for their use where needed, which is the case in very shallow water (from the tsunami point of view). In addition, we are interested in this study on near-field tsunamis, that is, those whose propagation distance is less than 1000 km. Henceforth, Cartesian coordinates can be used. The vertically integrated governing equations are then (Dean and Dalrymple, 1984, equations 5.13, 5.16, and 5.17, after setting the momentum correction factors equal to unity, and neglecting the horizontal shear stresses)

$$\frac{\partial \eta}{\partial t} + \frac{\partial M}{\partial x} + \frac{\partial N}{\partial y} = 0$$

$$\frac{\partial M}{\partial t} + \frac{\partial}{\partial x}\left(\frac{M^2}{D}\right) + \frac{\partial}{\partial y}\left(\frac{MN}{D}\right) + gD\frac{\partial \eta}{\partial x} + \frac{gn^2}{D^{7/3}} M\sqrt{M^2+N^2} = 0 \qquad (1.a,b,c)$$

$$\frac{\partial N}{\partial t} + \frac{\partial}{\partial x}\left(\frac{MN}{D}\right) + \frac{\partial}{\partial y}\left(\frac{N^2}{D}\right) + gD\frac{\partial \eta}{\partial y} + \frac{gn^2}{D^{7/3}} N\sqrt{M^2+N^2} = 0$$

where

$$M = U\,(h + \eta) = U\,D, \qquad N = V\,(h + \eta) = V\,D \qquad \textbf{(2)}$$

(M, N) are discharge fluxes, (U,V) are the vertically averaged horizontal particle velocities, g is the gravitational acceleration, h is still water depth, η the vertical displacement of the water surface above the still water level ($z = 0$), D is the total water depth ($h + \eta$), and n is Manning's roughness coefficient.

For completeness, the way the bottom friction terms are represented in Equations 1 is explained briefly. After the vertical integration the friction terms appear as τ_{bx}/ρ and τ_{by}/ρ in the x and y momentum equations, respectively, where ρ is the water density. The most widely used roughness factor coefficient is the so-called Manning's n [T/L$^{1/3}$], in which case the bottom friction, τ_b, is expressed as

$$\tau_{bx} = \frac{\rho\, g\, n^2}{\delta\, D^{1/3}}\, U\, |U^2 + V^2|^{1/2}; \quad \tau_{by} = \frac{\rho\, g\, n^2}{\delta\, D^{1/3}}\, V\, |U^2 + V^2|^{1/2} \qquad \textbf{(3)}$$

where δ has the value of unity for SI units and 1.49 for English units. After substituting for M and N from equation (2) we get the friction terms as shown in equations (1.a,b,c).

Notice that there is no Coriolis term which is a valid approximation for near-field tsunamis, but not for trans-oceanic, or far-field, ones (Goto and Ogawa, 1992; Kowalik and Whitmore, 1991). Kowalik and Whitmore (1991) demonstrated that even for propagation distances encompassing an east-west displacement as large as 30 degrees, the Coriolis term is not important.

For the simulation reported here n has been set equal to 0.025. It can also be made a function of position, in which case an array of values should be supplied to be read during execution, allowing for better match of observations and results, but this was not done.

The time evolution of the bottom displacement is not included in the continuity equation of the ocean layer since, as explained above, the vertical sea bottom displacement is assumed to occur instantaneously and simultaneously at every depth point across the zone affected by the fault movement.

In the simulations discussed in this study the nonlinear terms are kept only for the computations performed in the inner, higher resolution, Grid C. Computer limitations precluded its inclusion in the intermediate resolution, Grid B. The model was run on a Silicon Graphics workstation, with 192 MB of RAM.

The above set of equations are solved by finite differences, as discussed in the Goto and Ogawa report. A leap-frog scheme is used, with truncation error of the second order. But prior to execution of the program tests have to be made based on the maximum ocean depths and minimum grid size in order to decide upon an optimum, but safe, value of the time increment according to the Courant, Friedrichs, and Lewy (CFL) condition, $\Delta t \leq \Delta x/(gh_{max})^{1/2}$. This Δt is kept the same for all the grids. Hence for Δx we use the size of the cells in Grid C, and for h_{max} the maximum depth in this same grid.

One of the most important capabilities of the Goto and Ogawa model is the inclusion of wave runup estimates. As stated above, runup is only taken into consideration in nonlinear computations, that is, where the nonlinear field acceleration terms are kept. In the linear mode, since no runup computation is done, the computation is not carried out for water depths shallower than 20 m, and vertical walls are set in place of the actual bottom slope. In the non-linear mode, whether a computation cell is considered dry or submerged depends on the total water depth, as follows (according to the sign convention of the model, all original elevations below mean sea level are positive - i.e., bottom depths are positive - while all original elevations above mean sea level are considered negative - i.e. all original elevations above mean sea level are negative)

$D = h + \eta > 0$, the cell is submerged, and
$D = h + \eta \, , 0$, the cell is dry.

A wave front is located between the dry and submerged cells. The discharge flux across the boundary between the two cells is computed if the ground height in the dry cell is lower than the

water level in the submerged cell. In other cases, the discharge flux is considered zero.

It should also be added that the astronomical tide is assumed as constant throughout the tsunami computation. In addition to simulating the sea surface displacement due to the tsunami, the model is also capable of computing the depth integrated horizontal velocities, but this option has not been used in this study.

The model output consists of three basic results:

1. Snapshots of the sea surface displacement all over the grid at given time intervals. Snapshots can be produced for each one of the nested grids. In this study results were output every minute, and a video movie has been prepared for both scenarios described above.

2. An array of the maximum sea surface displacement at each grid cell independently of the time when it occurred. This array is the one used to examine the maximum runups in the grids where the model is used in its non-linear mode.

3. Time histories of sea surface elevation at selected grid points.

8. DISCUSSION OF RESULTS

Figure 5 shows snapshots of the surface displacement at times $t = 0$ (initial condition), 3, 6, and 9 minutes. The initial sea surface displacement was positive towards Puerto Rico, and this is manifested in that at all sites along the west and north coast of the island the model's time histories show a relatively small (less than a meter) surface elevation as the first tsunami signal, a signal that at some locations would be practically undetectable from the normal sea surface variability at the sites in the relatively steep topography of Puerto Rico's coastline region. This initial positive sea surface elevation becomes less noticeable the farther we move from the source. The initial disturbance has a quadrupole structure, the crest being slightly higher along the northern than along the southern side ($\approx$ 0.69 m vs. $\approx$ 0.48 cm), and the trough along the northern side being slightly shallower than along the southern side ($\approx$ - 1.35 m vs. $\approx$ -1.98 m). A movie of the simulation (90 min) is available through the Internet at site http://rmocfis.upr.clu.edu/~tsunami.

The figure shows how the wave front is deformed by the faster propagation speed along the Puerto Rico Trench. Travel times match very well the observed ones. For example, at Aguadilla the model results (Figure 6 shows the time histories at the sites for which estimates are available from the Reid and Taber 1919 report) show the initial crest maximum (approximately 0.75 m high) reaching the coast at $t \approx 6$ minutes, followed by a relatively broad and deep trough (3 m at its minimum) between t $\approx$ 6 and 8 min. As quoted above, estimates of the arrival of the "sea wave" vary between 4 and 7 minutes, although it is not clear at this, and other, sites if they are describing the crest or the trough of the "sea wave". At Mayaguez the Reid and Taber observations quote an arrival time of "the sea wave" varying between 23 and 30 minutes. The time history for Mayaguez shows sea level starting to rise at approximately 14 minutes, reaching a

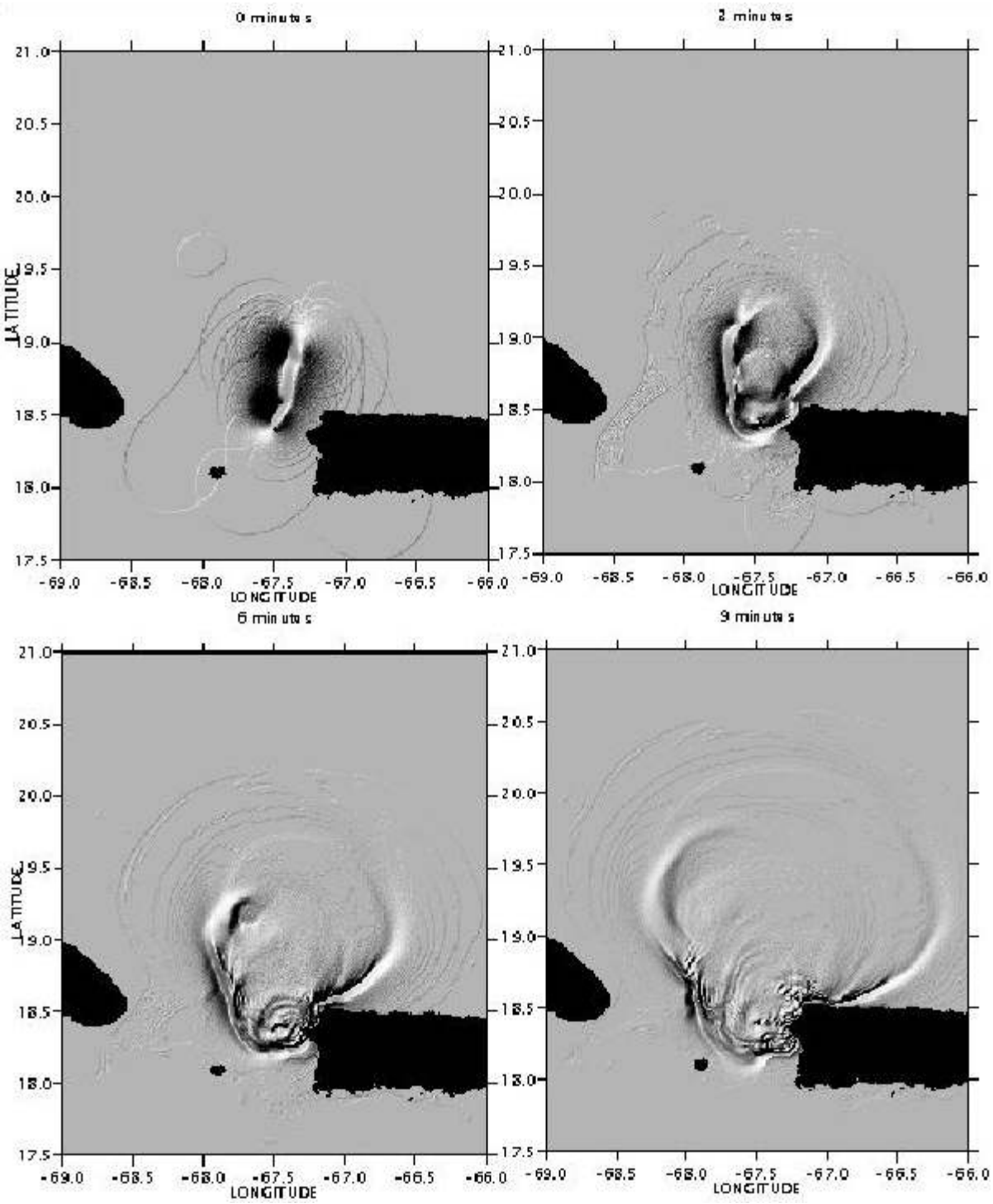

Figure 5 Snapshots of tsunami propagation at times 0,3,6,9 minutes.

maximum (≈ 0.4 m) and rapidly decreasing to a minimum of approximately 2 m at t = 23 minutes, followed by the arrival of a crest twice the height of the initial crest (≈ 0.8 m) at t ≈ 30 minutes. Finally, at Boquerón Bay the model's time history shows what should have been almost imperceptible sea level fluctuations followed by a sea level retreat starting at t ≈ 43 minutes and lasting until t ≈ 49 minutes. According to the Reid and Taber report quoted above, it took about 45 minutes for the wave to be felt at this bay.

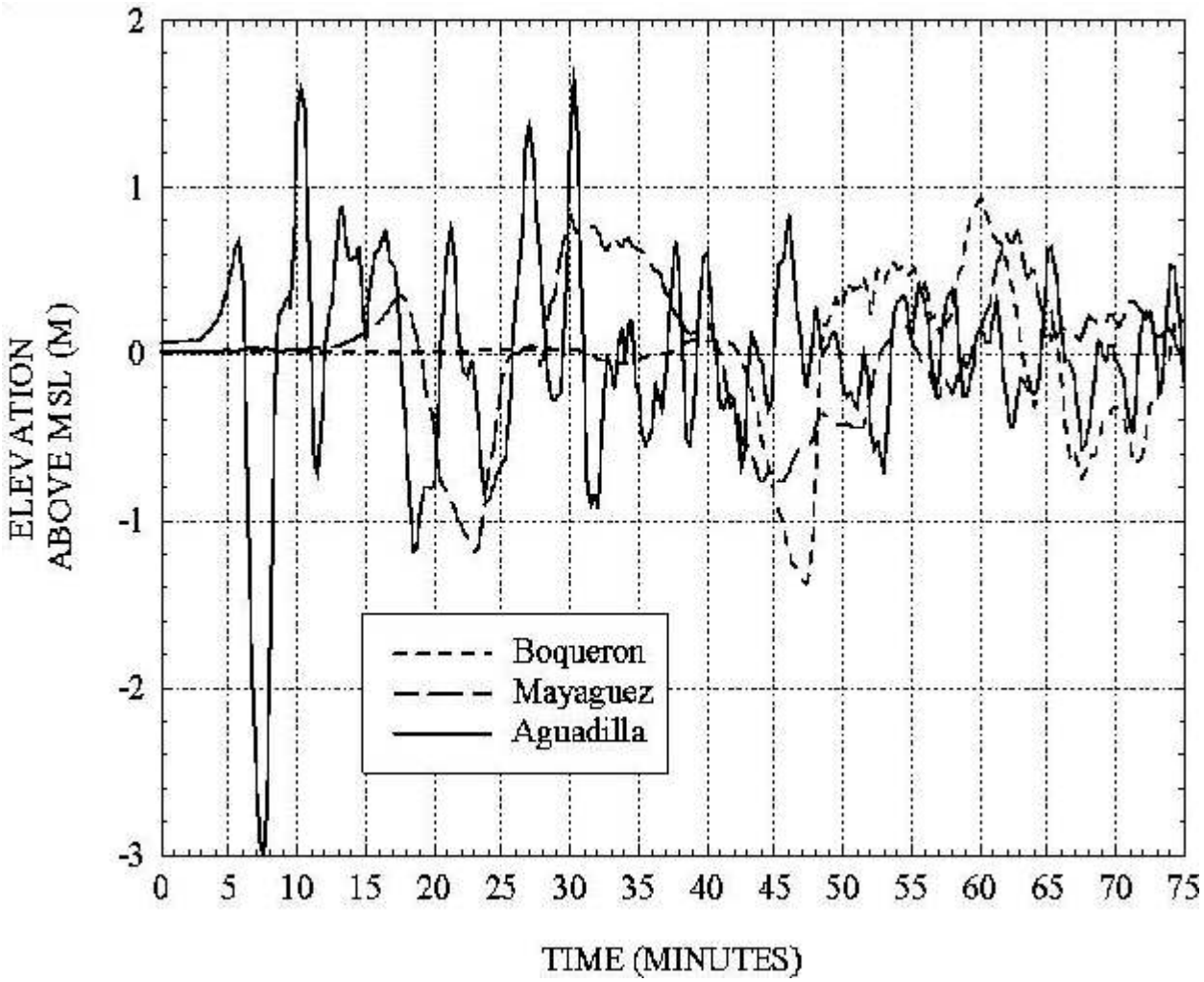

Figure 6 Time histories of sea surface elevation at sites for which observations were available.

Figure 7 shows a plot of the simulated maximum runup all along the west coast of Puerto Rico (left vertical axis). Also shown in the same plot is the coastline of the western part of the island (right vertical axis), together with the Reid and Taber (1919) measurements and observations at the highest runups and , within the limitations due to a 3 arc-sec resolution (approximately 90 m), it has quantitatively matched these elevations reasonably well.

Finally, Figure 8 shows the predicted flooding in the area of the city of Aguadilla, the one most affected. This is the final product that this pilot study was supposed to produce.

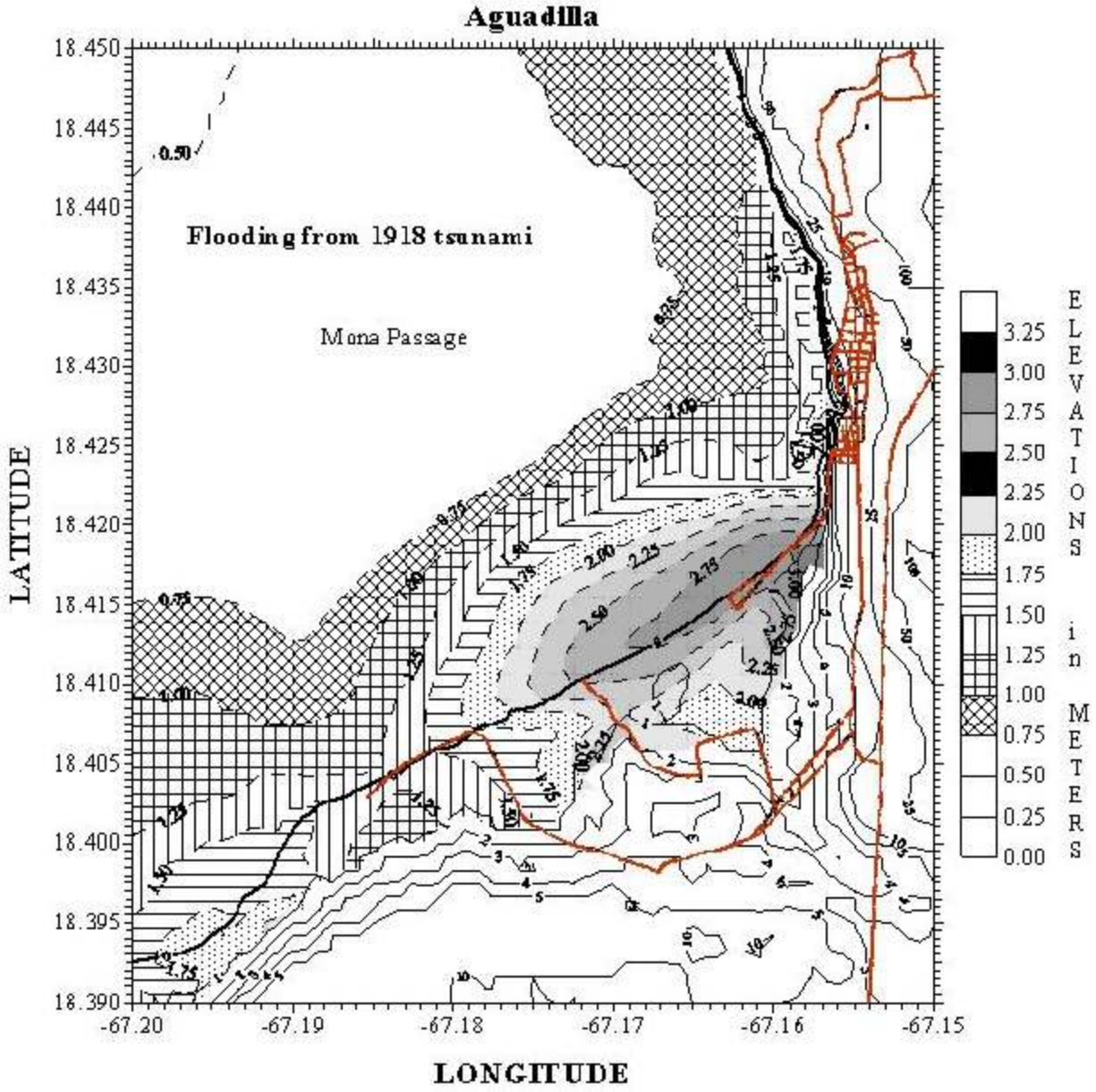

Figure 7 Flood map for the city of Aguadilla for 1918 tsunami based on the numerical simulation. Shoreline is the zeroelevation contoure. Terrain elevation contours are solid; sea surface elevation contours are dashed. Some city streets and roads are also shown.

9. CONCLUSION

The application of a tsunami generation, propagation, and runup, model (obtained through the TIME project) to the 1918 Puerto Rico tsunami has led to a relatively successful simulation of one of the most damaging tsunamis in the Caribbean Sea. In a qualitative way the model has highlighted the areas along the west coast of the island where the maximum runups were observed. But also in a quantitative way the model has matched relatively well the observed runup elevations given the obvious limitations due to the topographic resolution (about 90 m) available. The importance of good bathymetric resolution has been highlighted by many researchers, most recently by Titov and Synolakis (1997).

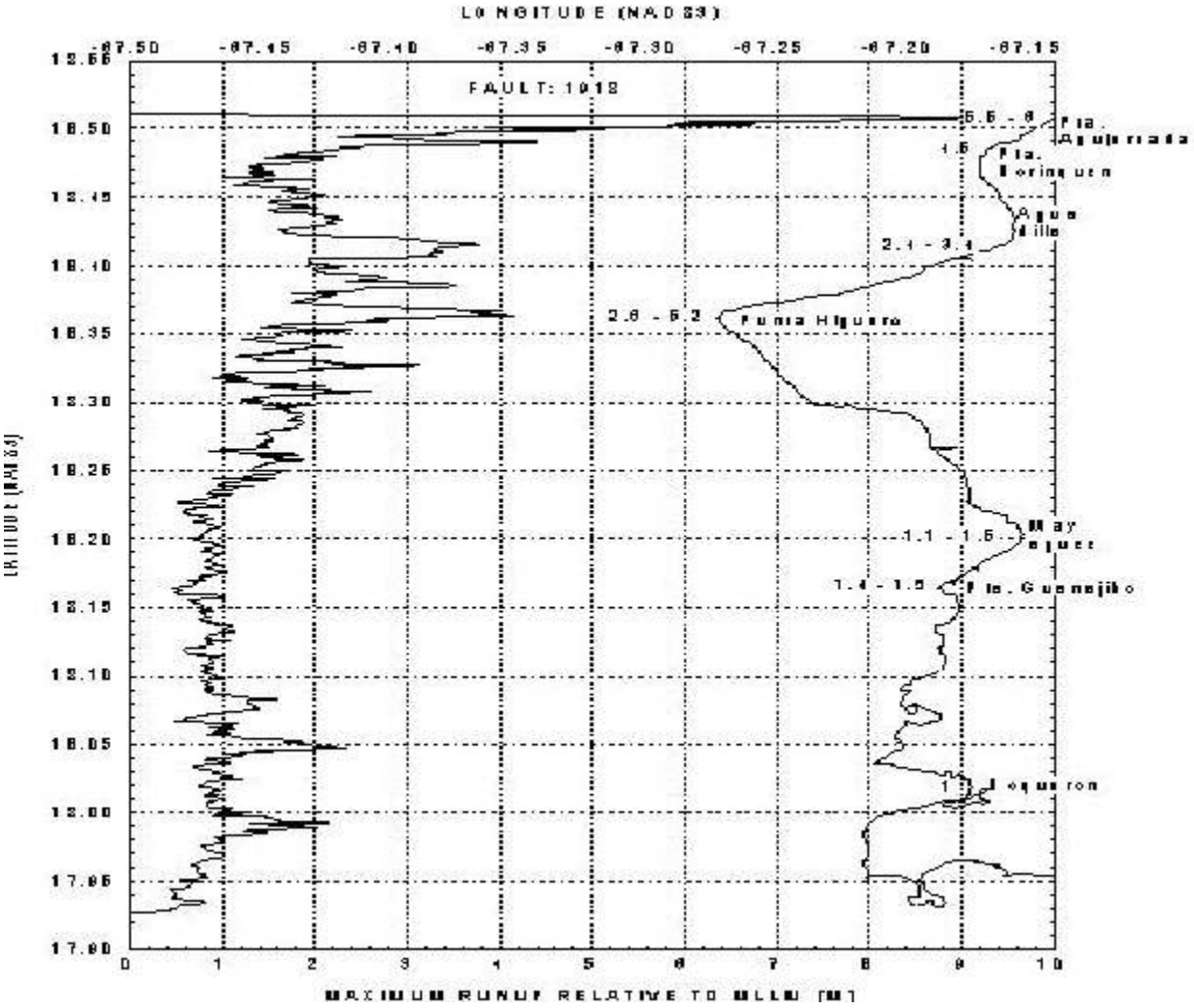

Figure 8 Runup distribution along west coast of Puerto Rico. Also shown are the observed values, from Reid and Taber (1919).

There is an additional source of uncertainty that will reflect on the exact location, and magnitude, of the maximum runups, specially in a coastline as complex as Puerto Rico's. This is related with he uncertainties in the fault parameters. The sensitivity of results as shown in Figure 8 to uncertainties in fault parameters is a topic of further on-going research.

ACKNOWLEDGMENTS

Both authors would like to acknowledge the assistance of Prof. Modesto Ortiz, of the Center for Stcientific Research and Higher Education of Ensenada, Mexico, who kindly spent two weeks in Puerto Rico as part of the TIME project for Puerto Rico. Mr. Harry Justiniano, Department of Marine Sciences, University of Puerto Rico, helped in the preparation of some of the graphs andthe movie. The financial assistance of the Puerto Rico Civil Defense and the Federal Emergency Management Agency (USA) is also acknowledged.

REFERENCES

Aki, K., and P. G. Richards, 1980. Quantitative Seismology. Vol. 1. W. H. Freeman, San Francisco. 575 pages.

Byrne, D. B.,, and W. McCann, 1985. Muertos Trough subduction - microplate tectonics in the northern Caribbean. *Nature*, Vol. 317:420-421.

Dean, R. G., and R. A. Dalrymple, 1984. Water Wave Mechanics for Engineers and Scientists. World Scientific Publishing Co., Singapore, 353 pp.

Demets, C., 1993. Earthquake slip vectors and estimates of present-day plate motions, *J. Geophys. Res.*, Vol. 98: 6703-6714.

Deng, J., and L. R. Sykes, 1995. Determination of Euler pole for contemporary relative motion of Caribbean and North American plates using slip vectors of interplate earthquakes. *Tectonics*, Vol. 14, No. 1: 39-53.

Goto, C. and Y. Ogawa, 1992. Numerical Method of Tsunami Simulation with the Leap-frog Scheme. Dept. of Civil Engineering, Tohoku University. Translated for the TIME Project by N. Shuto.

Kowalik, Z., and P. M. Whitmore, 1991. An investigation of two tsunamis recorded at Adak, Alaska. *Science of Tsunami Hazard*, Vol. 9, No. 2: 67-83.

Lander, J., 1997. Caribbean tsunamis: an initial history. Presented at the Caribbean Tsunami Workshop, June 11-13. Sponsored by Sea Grant College Program, University of Puerto Rico.

Masinha, L., and D. E. Smylie, 1971. The displacement fields of inclined faults. *Bull. Seismological Soc. America*, Vol. 61, No. 5:1433-1440.

Mason, D. G., and K. M. Scanlon, 1991. The neotectonic setting of Puerto Rico. *Geol. Soc. America Bull.*, Vol. 103: 144-154.

Mercado, A., 1994. Digitization of National Ocean Survey Hydrographic "Smooth" Sheets for Puerto Rico and the U.S. Virgin Islands. Submitted to Sea Grant College Program, University of Puerto Rico. 116 p.

Ramming, H. G., and Z. Kowalik. 1980. Numerical Modelling of Marine Hydrodynamics. Elsevier, New York, 368 pp.

Reid, H. F. and Taber, S., 1919. The Porto Rico earthquake of 1918. House of Representatives, 66th Congress, 1st Session. Document No. 269. November 19, 1919.

Shuto, N., T. Suzuki, K. Hasegawa, and K. Inagaki, 1985. Summary of a study of numerical techniques on the tsunami propagation and run-up. Proc. Int. Symp., eds. T. S. Murty and

W. J. Rapatz, Inst. Ocean Science, B. C., Canada, 88-92.

Shuto, N., T. Suzuki, K. Hasegawa, and K. Inagaki, 1986. A study of numerical techniques on the tsunami propagation and run-up. *Science of Tsunami Hazard*, Vol. 4: 111-124.

Shuto, N., 1991. Numerical simulations of tsunamis - its present and near future. *Natural Hazards*, Vol. 4: 171-191.

Slemmons, D. B., and C. M. Polo, 1992. Evaluation of acting faulting and associated hazards. In Studies in Geophysics, Active Tectonics. Pp. 45-62, National Academy Press, Washington. D.C.

Sykes, L. R., W. McCann, and A. Kafka, 1982. Motion of Caribbean plate during the last 7 million years and implications for earlier cenozonic movements. *J. Geophys. Res*., Vol. 70: 5065-5074.

Titov, V. V., and C. E. Synolakis, 1997. Extreme inundation flows during the Hokkaido-Nansei-Oki tsunami. *Geophys. Res. Lett.*, 24, No. 11: 1315-1318.